Journal of Geophysical Research: Solid Earth

Supporting Information for

Reconciling Estimates of Mantle Viscoelasticity via the Complex Viscosity: cases from Antarctica and Western USA

H.C.P. Lau[1], J. Austermann[2], B.K. Holtzman[2], C. Book[1], C. Havlin[3], Emily Hopper[2], and A.J. Lloyd[2]

[1]Earth and Planetary Science, University of California, Berkeley. CA. USA.

[2]Lamont-Doherty Earth Observatory, Columbia University, NY. USA.

[3]University of Illinois, Urbana-Champaign, IL. USA.

Corresponding author: Harriet C.P. Lau (hcplau@berkeley.edu)

Contents of this file

Introduction

The following material includes several supporting figures (Figs S1-S4), a supporting calculation and its explanation (Text S4), and a table summarizing the observations and the timescales assigned to them (Table S1).

Figure S1. Joint Posterior Probability Distributions of Thermodynamic Conditions

For each region **(a-c)**, the subpanels (i-iii) display the joint posterior probability distributions (top panels) for fitting v_s within the asthenosphere (shaded bar in Fig. 5(a-c), subpanels (i-ii)) as a function of temperature, T, within that shaded region, grainsize, g, and melt fraction ϕ. The green dot is the maximum posterior probability. Subpanels (iv) display the posterior probability distribution of the thickness of the conductive lid, z_{LID}.

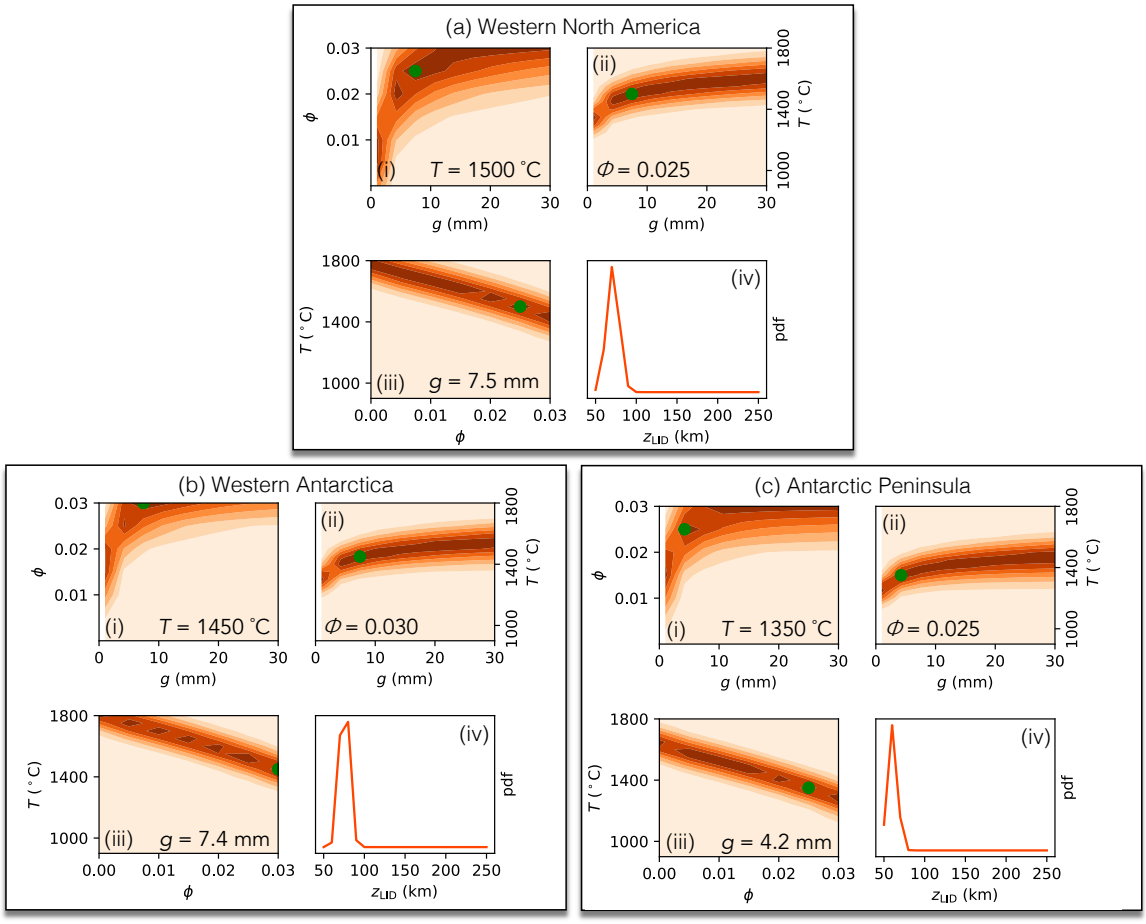

Figure S2. Additional Dissipation Parameters for Western North America and Antarctica Regions

Panels **(a-c)** are dissipation parameters for the regions Western North America, Western Antarctica, and Antarctic Peninsula, respectively. In all, the top panels show the complex modulus, M^*, where the solid likes are the real part (left vertical axis) and the dashed lines are the imaginary part (right vertical axis). The middle panels show the attenuation, or inverse quality factor, Q^{-1}, and the bottom panels show the quantity $\bar{\eta}^*$ (derived in Lau & Holtzman, 2019). Departures from unity in this quantity highlights the contribution of transient dissipation to the combined constitutive laws. The horizontal axes are shared by all panels, where frequency, f, is indicated by the bottom axes and the timescale is indicated by the top axes.

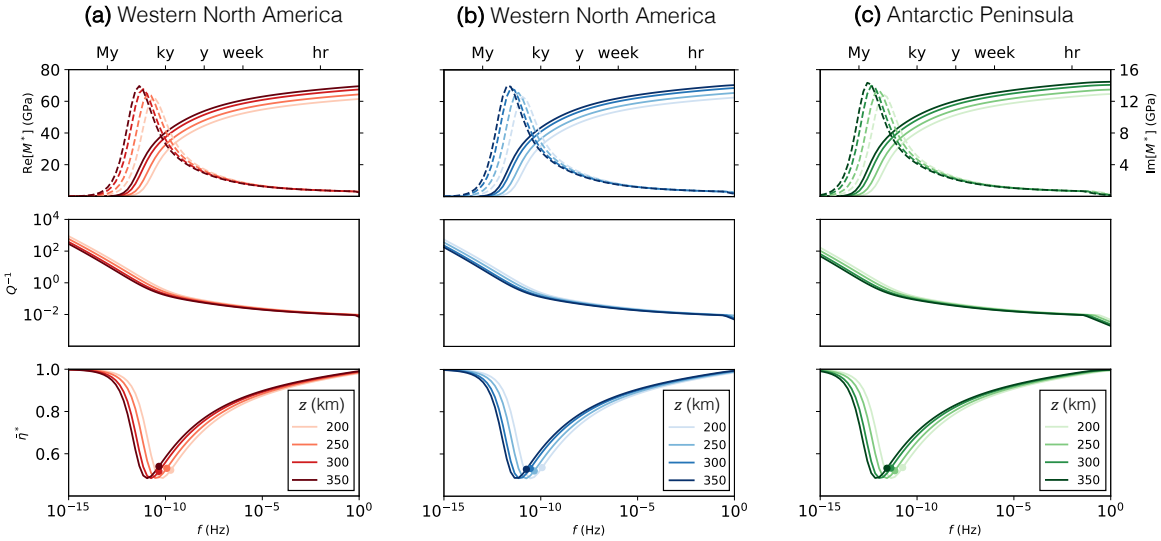

Figure S3. Apparent Quantities using other Constitutive Laws

For each region, **(a)-(c)**, we have placed predictions of steady state viscosity (top subpanels), apparent lithospheric thickness (middle subpanels), and apparent asthenospheric viscosity (bottom subpanels), from the combined constitutive laws of: MacCarthy et al. (2011) (thick black line, as in Main Text); the Extended Burgers model of Faul and Jackson (2015) (solid colored lines); and the Relaxation Spectrum Fit of Takei (2017) with premelt effects (though melt-free) (dashed colored lines). These are analogous to Fig. 5 (Main Text) though we have not included the effects of steady state dislocation.

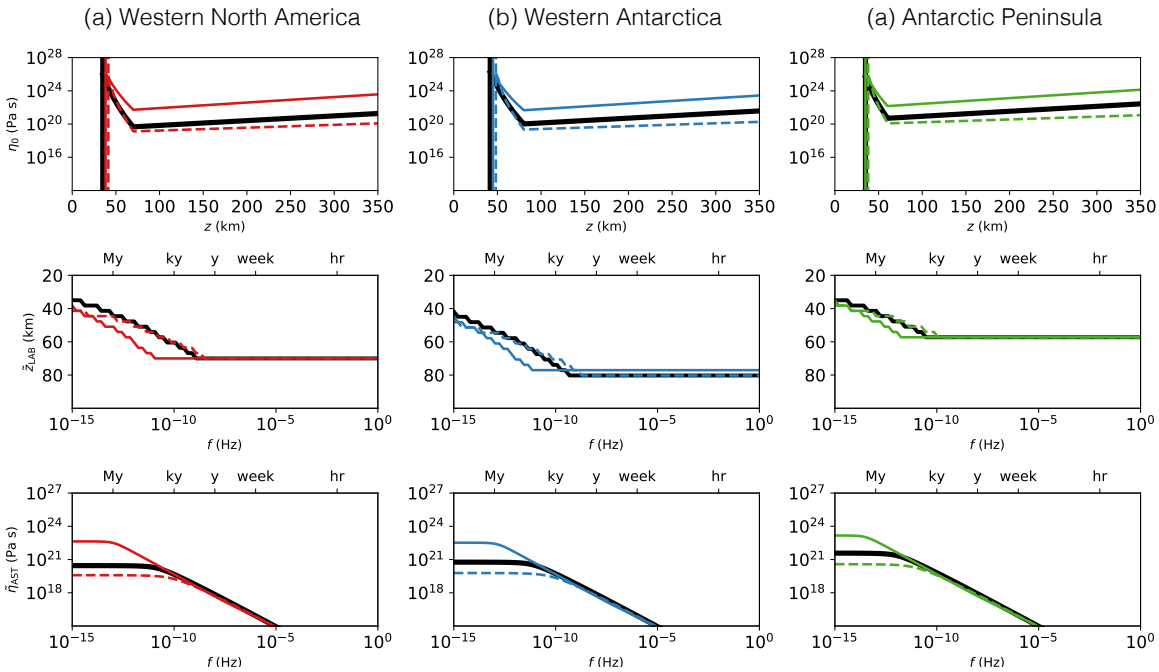

Text S4: Stress Evolution during GIA

To demonstrate the stress levels that can be reached in the asthenosphere, we perform a simple viscoelastic loading calculation adopting a Maxwell viscoelastic model. We use the formulation of Mitrovica & Milne (2003) though with simplifications: we assume longitudinal symmetry, no rotation, and that we only calculate solid earth deformation in response to ice growth (i.e., we do not consider the effects of the ocean); and thus only focus on the vicinity of the ice sheet. The input parameters include the elastic and density profile of PREM (Dziewonski & Anderson, 1981). We impose a lithosphere of 200 km thickness and values of $\boldsymbol{\eta_0}$ of 5×10^{20} Pa s and 5×10^{21} Pa s across the upper mantle (200 to 670 km depth) and lower mantle (670 to 2900 km depth), respectively. The growth of an ice sheet of 1,000 m over ~ 5,000 years results in stress levels within the lithosphere and asthenosphere that reach ~MPa – sufficient to induce changes in dislocation structure. The results are summarized in Fig. S4.

Figure S4. Stress Evolution during GIA

(a) Maximum ice height as a function of time. **(b)** Ice profiles as a function of distance from the North Pole (x). Each line represents the profile at a given time indicated by the colorbar. The solid black lines are the associated bedrock elevations. **(c)** The stress profiles at different depth, z, slices, as a function of x. Each line represents the stress profile at a given time indicated by the color bar.

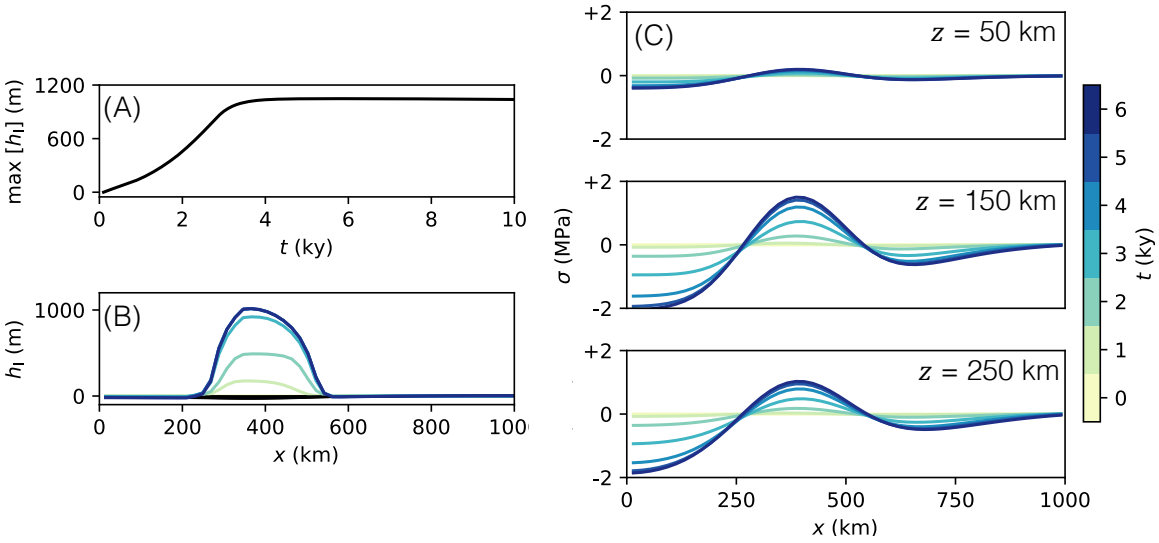

Table S1: Timescales Assigned to Observations

Tabulation of all the assigned values of τ_{dur} and τ_{del} for each observation and the associated explanation. For each value of τ_{dur} and τ_{del} listed, we consider ±20% of these values also.

Reference	Region	Process	τ_{dur}; τ_{del}	Comments
Creveling et al. (2017)	W-NA	GIA	20,000 y; 5,000 y	GIA during Marine Isotope Stages 5a and 5c: the timing between these events (and associated glacial-interglacial load changes) is around 20,000 y; sea level is recorded over the course of the interstadial by sea level indicators across W-NA.
Austermann et al. (2020)	W-NA	Lake rebound	4,000 y; 0 y	Loading of lake Bonneville over a duration of ~4,000 y (prior its rapid unloading ~14 ky BP), as recorded by paleoshorelines synchronously with unloading.
Pollitz et al. (2000)	W-NA	Postseismic Relaxation	0.1 y; 3 y	1992 Landers earthquake and the relaxation measured by GPS three years following.
Dickinson-Lovell et al. (2018)	W-NA	Postseismic Relaxation	0.1 y; 0 y	2010 El Mayor-Cucapah earthquake and the relaxation measured by GPS immediately after.
Barletta et al. (2018)	W-ANT	GIA	102 y and 12 y; 0 y	Ice change in the Amundsen Bay region with two rates of ice loss between 1900-2002 and 2002-2014, measured from 2002 onwards.
Wolstencroft et al. (2015)	ANT-P	GIA	15,000 y; 5,000 y	Last glacial maximum, ~21,000 y BP, to ~6,000 y BP with deformation measured by GPS today.
Ivins et al. (2011)	ANT-P	GIA	200 y and 80 y; 700 y and 70 y	Deformation from the Little Ice Age (1030 CE – 1300 CE) and modern ice mass chance (1850 – 1930) recorded by GPS over a duration of 1993-2007.
Nield et al. (2015)	ANT-P	GIA	10 y; 7 y	Collapse of Larsen B ice shelf between 1993-2002, recorded by GPS stations from 2009.
Samrat et al. (2020)	ANT-P	GIA	15 y; 7 y	Ice mass loss of Larsen A and B ice shelves measured by GPS extended to up to 2018 from Nield et al. (*3*).